Eur. Phys. J. D (2016) 70: 124
DOI: 10.1140/epjd/e2016-70102-1

THE EUROPEAN PHYSICAL JOURNAL D

Regular Article

Electron scattering cross sections for the modelling of oxygen-containing plasmas*

Luís Lemos Alves[1,a], Philippe Coche[1], Marco Antonio Ridenti[2], and Vasco Guerra[1]

[1] Instituto de Plasmas e Fusão Nuclear, Instituto Superior Técnico, Universidade de Lisboa, Av. Rovisco Pais, 1049-001 Lisboa, Portugal
[2] Instituto Tecnológico da Aeronáutica, Departamento de Ciência e Tecnologia Aeroespacial, 12228-900, São José dos Campos, São Paulo, Brazil

Received 15 February 2016 / Received in final form 12 April 2016
Published online 2 June 2016 – © EDP Sciences, Società Italiana di Fisica, Springer-Verlag 2016

Abstract. This work proposes a set of electron scattering cross sections for molecular and atomic oxygen, with interest for the modelling of oxygen-containing plasmas. These cross sections, compiled for kinetic energies up to 1 keV, are part of the IST-LISBON database with LXCat, being used as input data to the LoKI (LisbOn KInetics) numerical code. The cross sections for ground-state molecular oxygen describe elastic and inelastic collision mechanisms, the latter including rotational excitations/de-excitations (treated using either a discrete or a continuous approach), vibrational and electronic excitations (including dissociation), dissociative attachment and ionisation. This set yields calculated swarm parameters that reproduce measurements within 5–20% (transport parameters) and within a factor of 2 difference (Townsend coefficients), for reduced electric fields in the range 10^{-3}–10^{3} Td. The cross sections describing the kinetics of atomic oxygen by electron-impact comprise elastic mechanisms, electronic excitation and ionisation from $O(^3P)$ ground-state, dissociation of O_2(X,a,b) (including dissociative ionisation and attachment) and of O_3, and detachment. These cross sections are indirectly validated, together with other elementary data for oxygen, by comparing the densities of $O((^4S^0)3p\ ^5P)$ obtained from the self-consistent modelling and from calibrated optical emission spectroscopy diagnostics of microwave-sustained micro-plasmas in dry air (80% N_2: 20% O_2), produced using a surface-wave excitation (2.45 GHz frequency) within a small radius capillary ($R = 345$ μm) at low pressure ($p = 300$ Pa). The calculated densities are in good qualitative agreement with measurements, overestimating them by a factor ∼1.5.

1 Introduction

Oxygen-containing low-temperature plasmas, often produced in combination with other molecular gases and/or with noble gases, are the focus of a wide-range of interests spanning from fundamental studies to applications in various fields, such as material processing and functionalisation [1,2], biomedical purposes [3–6] and environmental/energy applications [7]. The modelling of these plasmas requires reliable basic data, namely for the accurate description of the electron kinetics in a plasma environment where molecular dissociation is often important.

This work proposes a set of electron scattering cross sections for both molecular and atomic oxygen, which has been used in the modelling of oxygen-containing plasmas by the Group of Gas Discharges and Gaseous Electronics of *Instituto de Plasmas e Fusão Nuclear* with *Instituto Superior Técnico* (IST) in Lisbon. These cross sections, compiled for kinetic energies up to 1 keV, are (or will be shortly) part of the IST-LISBON database with LXCat [8,9], being used as input data to the LoKI (LisbOn KInetics) numerical code [10].

The LXCat project is an open-access website for collecting, displaying, and downloading electron and ion scattering cross sections for binary encounters (swarm-derived, measured or calculated using quantum mechanical theory), electron and ion swarm parameters (measured transport parameters and rate coefficients), interaction potentials, optical oscillator strengths and other data essential for modelling low-temperature plasmas. LXCat is organised in databases, contributed by members of the community around the world and indicated by the contributor's chosen title.

The LoKI code is an in-house simulation tool that couples two main calculation blocks to solve: (i) the homogeneous two-term electron Boltzmann equation (for a pure gas or a gas mixture, including first and second-kind collisions, as well as electron-electron collisions); (ii) the

* Contribution to the Topical Issue "Advances in Positron and Electron Scattering", edited by Paulo Limao-Vieira, Gustavo Garcia, E. Krishnakumar, James Sullivan, Hajime Tanuma and Zoran Petrovic.

[a] e-mail: llalves@tecnico.ulisboa.pt

system of zero-dimensional (volume averaged) rate balance equations for the most relevant charged and neutral species in the plasma.

The cross sections proposed here for electron collisions with O_2 ground-state constitute a complete and consistent set of elementary data. The set is *complete* because it is able to describe the main electronic processes responsible for momentum and energy losses, including those yielding changes in the number of electrons, such as ionisation and attachment. The set is *consistent* since it is able to reproduce measured values of swarm parameters when used as input data to evaluate the electron energy distribution function (EEDF) from a Boltzmann solver or Monte Carlo/Particle-in-Cell codes. The complete and consistent set of cross sections proposed in this work is defined adopting a swarm-based procedure [11,12], very popular in gaseous electronics. The procedure starts with the collection of a set of cross sections from the literature, whose magnitudes are adjusted (within experimental error or theoretical uncertainty, if possible) to improve the agreement between calculated and measured swarm data. Such procedure works only as a global consistency criterion for macroscopic electron parameters, considered highly meaningful for plasma modelling, but it does not validate the cross section of each individual process nor it ensures the uniqueness of the whole cross section set. Conversely, adopting very reliable cross sections for some individual mechanisms, obtained from key references such as the compilation by Itikawa [13] or the works of Laporta et al. [14,15], is not a relevant alternative because: (i) these works do not provide complete cross section sets and (ii) the updating of individual cross sections jeopardises the consistency check with swam parameters.

In this work, the set of e-O_2 cross sections is validated by using the two-term Boltzmann solver embedded in LoKI to calculate swarm parameters over a large range of reduced electric fields $E/N = 10^{-3}$–10^3 Td (E is the electric field; N is the gas density; 1 Td = 10^{-17} V cm^2), checking the agreement between the results obtained and the experimental data available. This analysis is done in Section 2, where we also address the need for a proper description of rotational excitation/de-excitation mechanisms in order to reproduce measured swarm data at very-low E/N values.

The study of electron-scattering cross sections for oxygen presented here involves also a comparison between the populations of atomic oxygen species obtained from the self-consistent modelling and from calibrated optical emission spectroscopy (OES) diagnostics of microwave-sustained micro-plasmas in dry air (80% N_2: 20% O_2), produced using a surface-wave excitation (2.45 GHz frequency) within a small radius capillary ($R = 345$ μm) at low pressure ($p = 300$ Pa). These extreme small-radius, low-pressure working conditions require very-high reduced electric fields for plasma maintenance, contributing to stimulate the electron kinetics, namely in the dissociation of oxygen, and thus providing an ideal testbed for the validation of electron-impact cross sections. Obviously, the study contributes to indirectly analyse the quality of the e-O_2 cross-sections, but primordially it gives a direct assessment of the e-O cross-section set proposed in this work. This analysis is presented in Section 3, where we briefly introduce the zero-dimensional (0D) kinetic model adopted, namely in what concerns the description of charged-particle transport. The paper closes with some final remarks in Section 4.

2 Electron cross sections for O_2

The IST-LISBON complete set of electron-scattering cross sections with ground-state molecular oxygen is represented in Figures 1a–1c, and it includes the following 14 mechanisms [16,17]: effective (elastic and inelastic) momentum-transfer, dissociative attachment and ionisation (see Fig. 1a); excitations to 4 vibrational levels (see Fig. 1b; note that the resonance structures with these cross sections were smoothed, since they have negligible effect on the electron kinetics calculations); and excitations to 7 electronic levels (a $^1\Delta_g$; b $^1\Sigma_g^+$; A $^3\Sigma_u^+$, C $^3\Delta_u$ and c $^1\Sigma_u^-$ bound states; A $^3\Sigma_u^+$, A' $^3\Delta_u$ and c $^1\Sigma_u^-$ yielding dissociation into $2O(^3P)$ and continuum Herzberg bands; B $^3\Sigma_u^-$ yielding dissociation into $O(^3P)+O(^1D)$ and continuum Schumann-Runge bands; and radiative levels with thresholds at 9.97 eV and 14.7 eV (see Fig. 1c).

In order to correctly describe the swarm parameters at very-low E/N, the set is further completed with the cross sections for the $J \longleftrightarrow J+2$ ($J = 1, 3, 5, \ldots, 29$) rotational excitation/de-excitation mechanisms. Here, we adopt the rotational cross sections proposed by Gerjuoy and Stein [18], deduced using the Born and the Born-Oppenheimer approximations in a multipole expansion of the electrostatic interaction integral, that retains only the quadrupole term. The choice for (long-range) quadrupole interactions is adequate for describing the electron scattering by non-dipolar molecules such as O_2, but the deduction of these cross sections assumes that the interactions occur at very-low kinetic energy ($u < 0.6$ eV), which might pose problems on the validity of the approach. On the other hand, the analytical expression of Gerjuoy and Stein is very convenient for carrying out a mathematical treatment of the collisional operator for rotations with the electron Boltzmann equation (see below), which justifies our choice of these cross sections. However, we have considered also the alternative set of rotational cross sections proposed by Oksyuk [19], deduced using the Born-Oppenheimer approximation. In this case, the inelastic scattering amplitudes are obtained from the elastic scattering amplitude calculated by Fisk [20]. The latter is based on the exact solution to Schrodinger's equation using an ad hoc potential separable in ellipsoidal coordinates. The approach is valid over a wide energy interval provided that Fisk calculations give reasonable results, which in practice corresponds to maximum kinetic energies of 1–10 eV. The quality of these collisional data is assessed not only by comparing calculations and measurements for several swarm parameters, but also by analysing the predictions given by the different cross sections for the electron power lost in the various collisional channels.

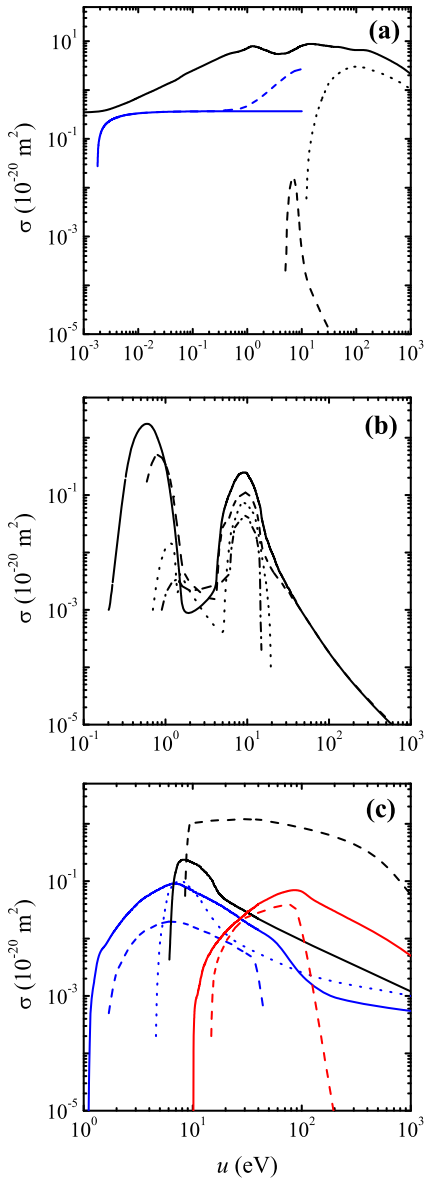

Fig. 1. Electron-neutral cross sections with the electronic ground-state of O_2. (a) Effective momentum-transfer (black solid line), dissociative attachment (black dashed), ionisation (black dotted), and $J = 1 \longrightarrow J' = 3$ rotational excitation from Gerjuoy and Stein [18] (blue solid) and from Oksyuk [19] (blue dashed). (b) Vibrational excitation from $v = 0$ to $v' = 1$ (solid line), $v' = 2$ (dashed), $v' = 3$ (dotted), and $v' = 4$ (dashed-dotted). (c) Electronic excitation to a $^1\Delta_g$ (blue solid line), b $^1\Sigma_g^+$ (blue dashed), A $^3\Sigma_u^+$ + C $^3\Delta_u$ + c $^1\Sigma_u^-$ bound (blue dotted), A $^3\Sigma_u^+$ + A' $^3\Delta_u$ + c $^1\Sigma_u^-$ dissociative (black solid), B $^3\Sigma_u^-$ dissociative (black dashed), and radiative levels at 9.97 eV (red solid) and 14.7 eV (red dashed).

As an example, Figure 1a plots the most intense electron-neutral rotational cross section, for the $J = 1 \longrightarrow J' = 3$ excitation, as proposed by Gerjuoy and Stein [18] and by Oksyuk [19].

As mentioned, the e-O_2 cross sections can be used as input data in the two-term Boltzmann solver with LoKI, to check their consistency by comparing calculation results with measurements available for swarm parameters. Because the study spans a large range of reduced electric-fields, the inclusion of rotational excitation/de-excitation mechanisms is needed in order to correctly account for the energy and momentum exchanges at very-low E/N. These mechanisms can be described simply by using the discrete form of the inelastic/superelastic collisional operator for rotations

$$J_{\rm rot} = N\sqrt{\frac{2e}{m}}\sum_J \delta_J \left[(u \pm u_{J,J\pm2}) \times\sigma_{J,J\pm2}(u \pm u_{J,J\pm2})f(u \pm u_{J,J\pm2}) - u\sigma_{J,J\pm2}(u)f(u)\right]. \quad (1)$$

In this equation, e and m are the electron charge and mass, respectively; u is the kinetic energy in eV; f is the EEDF satisfying the normalisation condition $\int_0^\infty f(u)\sqrt{u}du = 1$; $\sigma_{J,J\pm2}$ are the inelastic/superelastic rotational cross sections for the $J \longrightarrow J \pm 2$ excitations/de-excitations; $u_J \equiv BJ(J+1)$ is the excitation energy of rotational level J, with B the rotational constant; and $\delta_J \equiv n_J/N$ is the relative density of the rotational level J with absolute density n_J, assumed to follow a Boltzmann distribution at gas temperature T_g (k_B is the Boltzmann constant)

$$\delta_J \equiv \frac{n_J}{N} = \frac{p_J \exp\left[-eu_J/(k_BT_g)\right]}{Z}, \quad (2)$$

with $Z \equiv \sum_J p_J \exp\left[-eu_J/(k_BT_g)\right]$ the rotational partition function and $p_J = g_N(2J+1)$ the total multiplicity of level J ($g_N = 1$ being its nuclear multiplicity).

The summation in equation (1) must include a sufficiently high number of rotational excited levels, so as to ensure the adequate description of the energy exchanges between their populations. For oxygen, the number of levels required is around 30, which implies managing a large volume of data, and at small energy step for accuracy purposes, thus corresponding to a significant computational burden. The problem can be circumvented by replacing the discrete collisional operator (1) by a convenient continuous approximation for rotations (CAR), including a Chapman-Cowling (CC) corrective term proportional to the gas temperature. The CC-CAR expression, deduced considering the analytical expression of Gerjuoy and Stein cross sections, writes [21]

$$J_{\rm rot}^{\rm CC-CAR} \simeq \frac{d}{du}\left[N\sqrt{\frac{2e}{m}}4\sigma_0 Bu\left(f + \frac{k_BT_g}{e}\frac{df}{du}\right)\right], \quad (3)$$

where $\sigma_0 \equiv 8\pi Q^2 a_0^2/15$, with Q the quadrupole moment constant in ea_0^2 units and a_0 the Bohr radius. For O_2, we take here $B = 1.8 \times 10^{-4}$ eV and $Q = 1.4$ [22], the latter corresponding to an effective value of the quadrupole moment constant that adjusts the Gerjuoy and Stein cross sections in order to best fit the measured electron swarm parameters. Equation (3) can be used as an alternative approach to describe electron-neutral rotational excitations/de-excitations with minimal numerical complications.

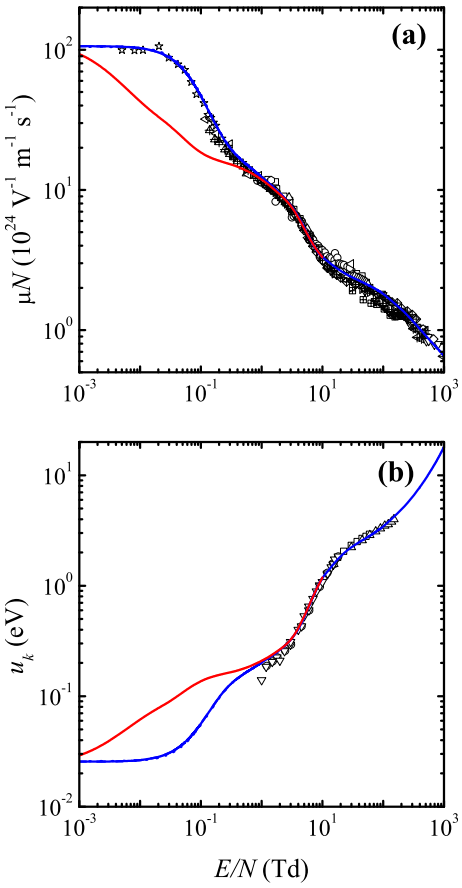

Fig. 2. Electron transport parameters in oxygen, as a function of the reduced electric field, for $T_g = 300$ K. The lines are calculation results obtained using the two-term Boltzmann solver with LoKI. For $E/N < 10$ Td, calculations include rotational encounters described according to the following approaches: discrete collisional operator, for rotational transitions up to level $J = 30$ with the Gerjuoy-Stein [18] (blue solid line) or the Oksyuk [19] (blue dashed) cross sections; CC-CAR (blue dotted); no rotational transitions (red). The points are experimental data, retrieved from the LXCat databases DUTTON [23] (open symbols) and LAPLACE [24] (crossed symbols). (a) Reduced mobility. The points are from the following authors: Nielsen and Bradbury [25] (□); Doehring [26] (○); Herreng [27] (△); Frommhold [28] (▽); Schlumbohm [29] (◇); Pack [30] (◁); Naidu and Prasad [31] (▷); Fleming et al. [32] (⊙); Nelson and Davis [33] (⋆); Brose [34] (⊞); Crompton and Elford [35] (⊕); Reid and Crompton [36] (⧋); Roznerski and Leja [37] (⧩); Jeon and Nakamura [38] (⧫); Lisovskiy et al. [39] (⧏). (b) Characteristic energy. The points are from the following authors: Huxley et al. [40] (□); Rees [41] (○); Naidu and Prasad [31] (△); Fleming et al. [32] (▽).

Figures 2a and 2b plot the reduced mobility μN and the characteristic energy $u_k \equiv \mu/D_e$ (with D_e the electron free-diffusion coefficient), respectively, as a function of E/N, calculated and measured in O_2 at $T_g \simeq 300$ K. Note that the various descriptions adopted for the rotational transitions yield similar results, depicted by almost coincident lines irrespectively of the fact that the simulations use the discrete approach, with the Gerjuoy and Stein or the Oksyuk cross sections, or the CC-CAR approach with a quadrupole moment constant $Q = 1.4$. Note further that the inclusion of rotational transitions is essential to reproduce the experimental values of the transport parameters for $E/N \lesssim 1$ Td. The results show that the set of cross sections proposed here yields good predictions of the electron transport parameters, when used as input data in a two-term Boltzmann solver. Indeed, the relative difference between calculations and measurements is below 20% for $E/N < 10$ Td and between 5–20% for $E/N > 10$ Td, against ≃40% dispersion in the experimental data.

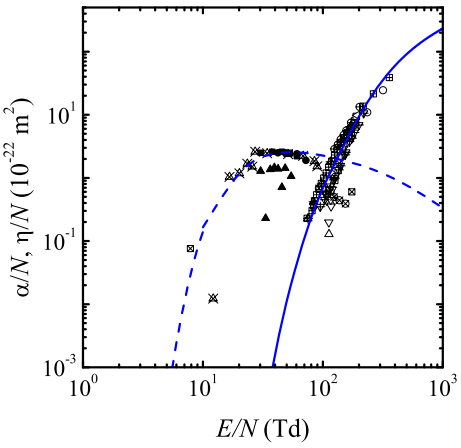

Fig. 3. Electron reduced Townsend coefficients in oxygen, as a function of the reduced electric field. The lines are calculation results, obtained using the two-term Boltzmann solver with LoKI, for the ionisation coefficient α/N (blue solid line) and the attachment coefficient η/N (dashed). The points are experimental data, retrieved from the LXCat databases DUTTON [23] (open/crossed (+) symbols) and LAPLACE [24] (filled/crossed (×) symbols). For α/N, the points are from the following authors: Harrison and Geballe [42] (□); Frommhold [43] (○); Prasad and Craggs [44] (△); Dutton et al. [45] (▽); Freely and Fisher [46] (◇); Schlumbohm [29] (◁); Price et al. [47] (⊞); O'Neill and Craggs [48] (⊕); Price et al. [49] (⧋); Corbin and Frommhold [50] (⧩). For η/N, the points are from the following authors: Huxley et al. [40] (■); Chatterton and Craggs [51] (●); Grünberg [52] (▲); Hake and Phelps [30] (⊠); Price et al. [49] (⊗); Lakshminarasimha et al. [53] (⧊).

Figure 3 plots calculations and measurements of the reduced Townsend coefficients in O_2, for ionisation α/N and for attachment η/N, as a function of E/N. Simulations differ from the measurements by a factor of 2, for η/N in the region 10–100 Td, and by a factor of 1.5, for α/N in the region 100–400 Td, again being found within the experimental uncertainty observed.

Figure 4 presents, as a function of E/N, the fractional power (relative to the electron power gained from the electric field) transferred to the different electron-collision mechanisms in O_2: elastic, rotational, vibrational and electronic. The results in this figure confirm the importance of rotational mechanisms in O_2 for $E/N \lesssim 0.5$ Td, where they are responsible for the majority of the electron power

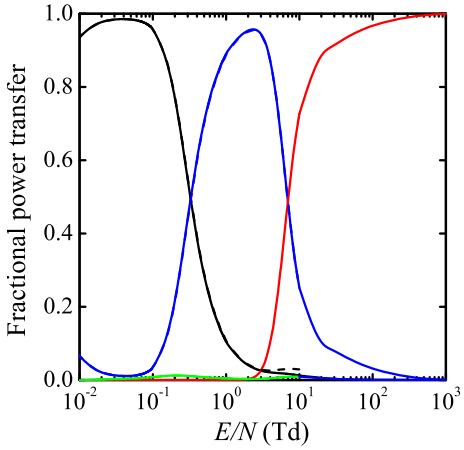

Fig. 4. Fractional power (relative to the electron power gained from the electric field), as a function of the reduced electric field, transferred to the following electron-collision channels in oxygen: elastic (green line), rotational (black), vibrational (blue) and electronic (red). The lines are calculations at $T_g = 300$ K, using the following approaches and data: for $E/N < 10$ Td, the discrete collisional operator for rotational transitions up to level $J = 30$, with the Gerjuoy-Stein [18] (solid lines) or the Oksyuk [19] (dashed) cross sections; for $E/N > 10$ Td, the CC-CAR operator.

losses, due to the very-low rotational characteristic temperature $\Theta_{\rm rot} \equiv (eB)/k_B \simeq 2.1$ K $\ll T_g$. Vibrational collisions are the dominant power-loss channel for $E/N \simeq$ 0.5–5 Td, after which the electron energy is dissipated mainly in electronic excitations. This result confirms the importance of vibrational mechanisms in the electron energy-budget, justifying the investment in developing state-resolved models including vibrationally excited O_2 molecules. The use of the Oksyuk cross sections (instead of Gerjuoy and Stein's) leads to negligible differences in the power transfer results, except for $E/N \simeq$ 5–10 Td where they yield a very small increase in the electron power lost in rotational collisions.

3 Electron cross sections for O

The set of electron-scattering cross sections with ground-state atomic oxygen O($2s^2 2p^4\ ^3$P) (represented in a more simplified notation as O(^{3}P)) is plotted in Figure 5a and it includes the following 8 cross sections [54]: elastic momentum-transfer; excitations to 6 electronic levels and ionisation. The electronic excited levels are: (i) O($2s^2 2p^4\ ^1$D), O($2s^2 2p^4\ ^1$S) and O($2s 2p^5\ ^3$P^0), represented as O(^{1}D), O(^{1}S) and O(^{3}P^0), respectively; (ii) the most important Rydberg states combined as follows: $3s\ ^5$S^0, $3p\ ^5$P, $4s\ ^3$S^0, $3d\ ^3$D^0, $4p\ ^3$P and $4d\ ^3$D^0 with core $2s^2 2p^3\ ^4$S^0, noted as O((^{4}S^0)nl); $3d\ ^3$S^0, $3d\ ^3$P^0, $3d\ ^3$D^0, $4d\ ^3$SPD^0 and $4s\ ^3$D^0 with core $2s^2 2p^3\ ^2$D^0, noted as O((^{2}D^0)nl); $3s\ ^3$P^0, $3d\ ^3$P^0 and $4s\ ^3$P^0 with core $2s^2 2p^3\ ^2$P^0, noted as O((^{2}P^0)nl). In the simplified notation, $n < 5$ and $l = s, p, d$.

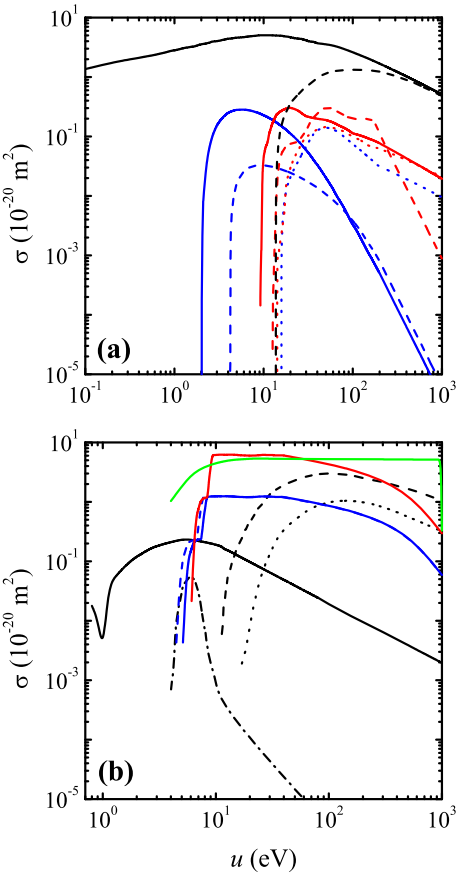

Fig. 5. Cross sections involving oxygen atoms. (a) Electron-impact collisions with the electronic ground-state of O: elastic momentum-transfer (black solid line) and ionisation (black dashed); electronic excitation to O(^{1}D) (blue solid), O(^{1}S) (blue dashed) and O(^{3}P^0) (blue dotted); electronic excitation to Rydberg states O((^{4}S^0)nl) (red solid), O((^{2}D^0)nl) (red dashed) and O((^{2}P^0)nl) (red dotted). (b) Collisions with electronic excited states, ozone and negative ion: $e + O_2(a) \longrightarrow e + O_2(b)$ (black solid line), $e + O_2(a) \longrightarrow 2e + O_2^+$ (black dashed), $e + O_2(a) \longrightarrow 2e + O^+ + O(^3P)$ (black dotted), and $e + O_2(a) \longrightarrow O^- + O$ (black dashed-dotted); $e + O_2(a) \longrightarrow e + 2O$ (blue solid) and $e + O_2(b) \longrightarrow e + 2O$ (blue dashed); $e + O_3 \longrightarrow e + O_2 + O$ (red); and $e + O^- \longrightarrow 2e + O(^3P)$ (green).

For the self-consistent modelling of air micro-plasmas at low pressure, these collisional data are complemented by the electron-impact cross sections represented in Figure 5b: excitation of b $^1\Sigma_g^+$ from a $^1\Delta_g$ [55] $e + O_2(a) \longrightarrow e + O_2(b)$; ionisation [17] $e + O_2(a) \longrightarrow 2e + O_2^+$ and dissociative ionisation $e + O_2(a) \longrightarrow 2e + O^+ + O(^3P)$ from a $^1\Delta_g$, the latter obtained by shifting the threshold of the corresponding ground-state cross section; dissociative attachment from a $^1\Delta_g$ [56] $e + O_2(a) \longrightarrow O^- + O$; dissociation from the a $^1\Delta_g$ and b $^1\Sigma_g^+$ excited states $e + O_2(a,b) \longrightarrow e + 2O$, obtained by threshold shift of the corresponding ground-state cross sections; dissociation of ozone [17] $e + O_3 \longrightarrow e + O_2 + O$; and detachment [57] $e + O^- \longrightarrow 2e + O(^3P)$.

The electron-scattering cross sections for oxygen adopted in this work are in part validated by comparing the absolute populations of atomic oxygen species, obtained from the self-consistent modelling and from calibrated OES diagnostics of microwave-sustained microplasmas in dry air (80% N_2: 20% O_2), produced using a surface-wave excitation (2.45 GHz frequency) within a small radius capillary ($R = 345$ μm) at low pressure ($p = 300$ Pa) [58,59]. The model adopts the very complete kinetic schemes presented in [60,61] for nitrogen and in [17,62] for oxygen and for N_2-O_2 mixtures. Note that the Rydberg species $O((^2P^0)nl)$, with excitation energy above the 13.61 eV ionisation threshold of $O((^4S^0)nl)$, is not included in the kinetic model, its creation being considered only as an electron energy-loss channel in the electron Boltzmann equation. In fact, O^+ is not the most important ion under our working conditions (see below) and moreover the electron-impact cross sections for the excitation of $O((^2P^0)nl)$ are found, near threshold, below those of the other Rydberg states. Note finally that the model has been further validated by comparing simulation results with measurements for the absolute populations of molecular nitrogen in electronic states $N_2(C,v')$ and $N_2^+(B)$ (agreement within factors of 2–3) and atomic nitrogen in electronic state $N(3p\ ^4S^0)$ (agreement within the experimental error bar) [58].

The modelling results are obtained with the LoKI code, using as input data the experimental values of the electron density ($n_e \simeq (1\text{–}4) \times 10^{12}$ cm^{-3}) and the gas temperature ($T_g \simeq 600$–1000 K) [58], in addition to the excitation frequency, the tube radius and the gas pressure. On output, calculations give the species densities and the reaction rates, calculating also the self-consistent reduced electric field E/N by imposing the quasi-neutrality condition, and adjusting the relative composition of the mixture after the dissociation of molecular species, while ensuring a constant pressure value. The code was originally designed to cover values of the product "pressure × radius" typically between 1 and 760 Torr cm, whereas here we have $pR = 0.08$ Torr cm, due to the small-radius low-pressure conditions adopted. Therefore, the code was adapted to correctly describe the transport of charged particles for the present working conditions [63], using the bases of the unified transport theory for dense plasmas at various pressures proposed by Self and Ewald [64], and later reinterpreted by Ferreira and Ricard [65]. The latter work expresses the results of Self and Ewald under the form of an effective diffusion coefficient D_{se} for electrons, which coincides with the classical ambipolar diffusion coefficient D_{ae} at high-pressure only, and analyses the variation of that coefficient with the gas pressure by plotting D_{se}/D_{ae} as a function of Λ/λ_+ (with Λ the characteristic diffusion length and λ_+ the ion mean-free-path). The main advantage of introducing the effective diffusion coefficient is because it allows writing the frequency of charged-particle transport losses as D_{se}/Λ^2, a very convenient form for using in 0D kinetic models.

The theory of Self and Ewald, initially developed for plasmas containing a single positive ion species, was revised so as to consider the presence of several positive ions and a negative ion with low density [63]. In particular, (i) the transport of the total positive charge in the plasma is described using a single effective positive ion; (ii) the model formulation is limited to low/intermediate pressures, considering vanishingly small attachment/detachment rates, in which case the low-density negative ion has negligible drift velocity and remains confined to the plasma core. Under these hypotheses, it is possible to retrieve a system of equations formally identical to that of [64], whose solution can be worked-out from the original results of Self and Ewald, yielding a correction upon the abacus D_{se}/D_{ae} vs. Λ/λ_+ given in [65].

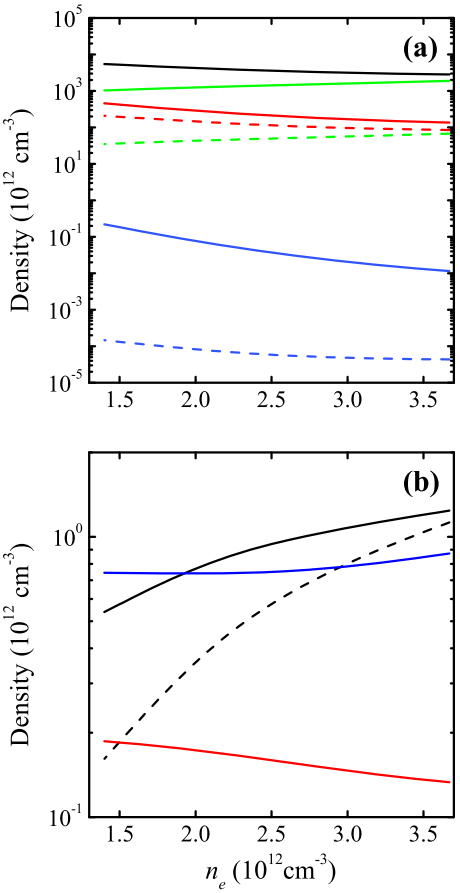

Fig. 6. Densities of oxygen species, as a function of the electron density, calculated using the LoKI code, for $p = 300$ Pa, $R = 345$ μm and a set of (n_e, T_g) values obtained from measurements [58]. (a) Molecular and atomic neutral species: $O_2(X)$ (black solid line); $O_2(a)$ (red solid) and $O_2(b)$ (red dashed); O_3 (blue solid) and $O_3^\star$ (blue dashed); $O(^3P)$ (green solid) and $O(^1D)$ (green dashed). (b) Ion species: O_2^+ (black solid line) and O^+ (black dashed); O^- (red); NO^+ (blue).

Figures 6a and 6b present, as a function of the electron density, the calculated densities of the oxygen neutral (molecular and atomic) and ion species, respectively. For completeness, the very important density of NO^+ is also shown in Figure 6b.

Figure 6a shows similar densities of $\sim 10^{15}$ cm^{-3} for the molecular and the atomic ground-states $O_2(X)$ and $O(^3P)$,

hence revealing a high dissociation degree for oxygen ($[O(^3P)]/[O_2(X)]$ ∼20%–70%). The excited species $O_2(a)$ and $O_2(b)$ have densities ∼ 10^{14} cm^{-3}, and the density of O_3 is 5–6 orders of magnitude below that of $O_2(X)$. The kinetics of the dominant molecular neutral species is controlled mainly by electron-impact excitation, ionisation and dissociation, which explains the decrease in the density of $O_2(X)$ when the electron density increases. The creation/destruction channels of $O_2(b)$ proceed also via the quenching of $O(^1D)$ with $O_2(X)$, and by diffusion and wall deactivation. The main creation channels of the atomic species are electron-impact dissociation and excitation, which explains the increase in their densities with n_e. The main destruction mechanism for these species is by diffusion and wall recombination/deactivation, for which we have considered a destruction coefficient $\gamma = 0.1$.

Figure 6b shows that O_2^+ and NO^+ are the most abundant ion species, with densities of ∼10^{12} cm^{-3}, followed by the atomic ion O^+ that can reach also a density of 10^{12} cm^{-3} at high n_e. Note that the population of the negative ion O^- is ∼10 times below the electron density, in agreement with the assumptions made to describe the transport of charged particles in the multicomponent plasma. The positive ion species are created mainly by electron-impact ionisation and are destroyed mainly by diffusion and wall recombination. The main creation/destruction mechanisms of the negative ion O^- are dissociative attachment and associative detachment, respectively.

Model results are compared with measurements of the absolute density of excited state $O(2s^22p^3\,(^4S^0)3p\ ^5P)$ [58]. Results are obtained from the triplet transitions at ∼777 nm wavelength (3.69×10^7 s^{-1} emission frequency), emitted from the three very-close sublevels of $O(2s^22p^3\ (^4S^0)3p\ ^5P)$ to $O(2s^22p^3\ (^4S^0)3s\ ^5S)$, represented in a more simplified notation as $O((^4S^0)3p\ ^5P) \longrightarrow O((^4S^0)3s\ ^5S)$. The experimental setup corresponds to a classical surface-wave discharge, produced within a capillary inserted into a wave launcher (surfatron). The latter is especially adapted to the system geometrical dimensions, ensuring a maximum electric field at the surfatron gap [66]. Dry air is introduced at negligible gas flow from the capillary open-end near the surfatron. The system generates stable plasmas with ∼3 cm length, ensuring constant pressure along the plasma column. Calibrated OES diagnostics are used to determine the absolute intensities of several radiative transitions (and also the electron density and the gas temperature). The measured spectra are calibrated using a standard tungsten lamp of known spectral radiance, and they are compared with Specair-simulated [67] spectra to obtain the absolute density of a particular excited state.

Figure 7 presents calculations and measurements of the density of $O((^4S^0)3p\ ^5P)$ excited state, as a function of the electron density. A corona model is used to estimate the population of this atomic state, taking into account its creation from the electron-impact excitation of $O(^3P)$ [54] and the electron-impact dissociation of $O_2(X)$ [68], and its destruction by electron-impact de-excitation [54], quenching with $O_2(X)$ [69] and radiative decay. Model predictions are in good qualitative agreement with measurements, overestimating them by a factor ∼1.5 (note that, in Fig. 7, the measured densities are multiplied by factor 1.54 for representation purposes), which in any case corresponds to values at the lower boundary of the error bars. In general, the model seems to embody the main features of the electron kinetics in oxygen, despite the typical uncertainties of its input data, namely those associated with the electron-impact cross sections.

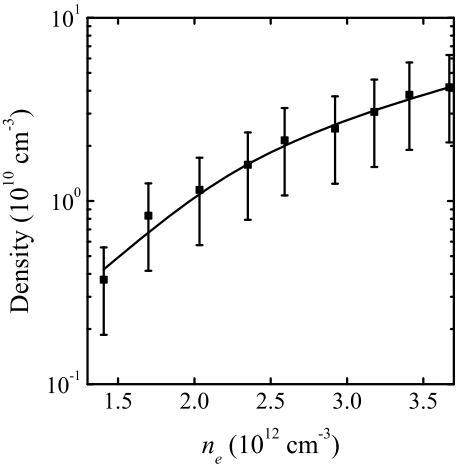

Fig. 7. Calculations (lines) and measurements (points) of the absolute density of atomic excited state $O((^4S^0)3p\ ^5P)$, as a function of the electron density. The measured densities [58] are multiplied by factor 1.54, becoming normalised to the corresponding calculated value at $n_e \simeq 3.7 \times 10^{12}$ cm^{-3}.

4 Final remarks

This work has proposed a set of electron scattering cross sections for both molecular and atomic oxygen, with interest for the modelling of oxygen-containing plasmas.

The cross sections for ground-state molecular oxygen describe elastic and inelastic collision mechanisms, the latter including rotational excitations/de-excitations, vibrational and electronic excitations (including dissociation), dissociative attachment and ionisation. When these cross sections are used as input data in a two-term Boltzmann solver, such as the one embedded in the LoKI (LisbOn KInetics) numerical code, they yield calculated swarm parameters that reproduce measurements within 5–20% (transport parameters) and within a factor of 2 difference (Townsend coefficients), for reduced electric fields in the range 10^{-3}–10^3 Td. Results show that the inclusion of rotational transitions is essential to reproduce the experimental values of the transport parameters for $E/N \lesssim 1$ Td. For this purpose, the rotational collision operator can be written using either a discrete description (e.g. considering the rotational cross sections proposed by Gerjuoy and Stein [18]) or a continuous approximation for rotations, duly corrected by a Chapman-Cowling term proportional to the rotational/gas temperature [21].

The cross sections describing the kinetics of atomic oxygen by electron-impact comprise elastic mechanisms, electronic excitation and ionisation from $O(^3P)$ ground-state, dissociation of O_2(X,a,b) (including dissociative ionisation and attachment) and of O_3, and detachment. These cross sections, complemented with other collisional data for oxygen (e.g. cross sections for excitation/de-excitation from O_2(a,b) and wall recombination/deactivation coefficients), were used in the LoKI code to model microwave-sustained micro-plasmas in dry air (80% N_2: 20% O_2), produced using a surface-wave excitation (2.45 GHz frequency) within a small radius capillary ($R = 345$ μm) at low pressure ($p = 300$ Pa). The code was adapted to correctly describe the transport of charged particles under the present small-radius low-pressure extreme conditions [63], using the bases of the unified transport theory for dense plasmas at various pressures proposed by Self and Ewald [64], and later reinterpreted by Ferreira and Ricard [65]. The update was extended to multi-component plasmas, composed by several positive ions and one negative ion with low density, and it yields a correction of ∼20% upon the charged-particle effective diffusion coefficient, for negative ion densities as low as $10^{-2}n_e$. The model (and the elementary data within it) was validated against measured values of the absolute intensities of several radiative transitions with $O^\star$, N_2 and $N^\star$, obtained using calibrated OES diagnostics. Model results for the density of the triplet excited state $O((^4S^0)3p\ ^5P)$ (∼777 nm wavelength transitions) are in good qualitative agreement with measurements, overestimating them by a factor ∼1.5.

The present work reveals that the current knowledge of electron scattering cross sections in oxygen already enables the modelling of oxygen-containing plasmas, to conclude about some aspects of their kinetic behaviour.

Model results can surely be improved by using updated elementary data for oxygen, namely e-O_2 cross sections for the vibrational excitation from ground-state $e + O_2(X,v) \leftrightarrow e + O_2(X,v')$ [14], electronic excitation from electronically [70] and vibrationally excited states, and state-specific dissociation from vibrationally excited $O_2(X,v)$ molecules [15]. The references proposing these data can provide invaluable contributions also in the assignment of cross sections to individual processes, for use on a Boltzmann solver. Work is in progress to update these data and assess their validity.

This work was partially supported by Portuguese FCT - Fundação para a Ciência e a Tecnologia, under Project UID/FIS/50010/2013. M.A. Ridenti acknowledges support from Coordenação de Aperfeiçoamento de Pessoal de Nível Superior under Grant CAPES/ITA 005/2014.

References

1. U. Cvelbar, K. Ostrikov, M. Mozetic, Nanotechnology **19**, 405605 (2008)
2. D. Mariotti, R.M. Sankaran, J. Phys. D **43**, 323001 (2010)
3. K. Kutasi, C.D. Pintassilgo, J. Loureiro, J. Phys.: Conf. Ser. **162**, 012008 (2009)
4. G.Y. Park, S.J. Park, M.Y. Choi, I.G. Koo, J.H. Byun, J.W. Hong, J.Y. Sim, G.J. Collins, J.K. Lee, Plasma Sources Sci. Technol. **21**, 043001 (2012)
5. J. Mizeraczyk, M. Dors, M. Jasiński, B. Hrycak, D. Czylkowski, Eur. Phys. J. Appl. Phys. **61**, 24309 (2013)
6. D. Graves, Phys. Plasmas **21**, 080901 (2014)
7. E. Tatarova, N. Bundaleska, J. Ph. Sarrette, C.M. Ferreira, Plasma Sources Sci. Technol. **23**, 063002 (2014)
8. L.L. Alves, J. Phys.: Conf. Ser. **565**, 012007 (2014)
9. IST-LISBON database, www.lxcat.net, retrieved on April 2015
10. V. Guerra, J. Loureiro, Plasma Sources Sci. Technol. **8**, 110 (1999)
11. Z.L. Petrović, S. Dujko, D. Marić, G. Malović, Ž. Nikitović, O. Šašić, J. Jovanović, V. Stojanović, M. Radmilović-Rađenović, J. Phys. D **42**, 194002 (2009)
12. L.L. Alves, K. Bartschat, S.F. Biagi, M.C. Bordage, L.C. Pitchford, C.M. Ferreira, G.J.M. Hagelaar, W.L. Morgan, S. Pancheshnyi, A.V. Phelps, V. Puech, O. Zatsarinny, J. Phys. D **46**, 334002 (2013)
13. Y. Itikawa, J Phys. Chem. Ref. Data **38**, 1 (2009)
14. V. Laporta, R. Celiberto, J. Tennyson, Plasma Sources Sci. Technol. **22**, 025001 (2013)
15. V. Laporta, R. Celiberto, J. Tennyson, Phys. Rev. A **91**, 012701 (2015)
16. A.V. Phelps, *Technical Report 28* (JILA Information Center Report, University of Colorado, Boulder, CO, USA, 1985)
17. G. Gousset, C.M. Ferreira, M. Pinheiro, P.A. Sá, M. Touzeau, M. Vialle, J. Loureiro, J. Phys. D **24**, 290 (1991)
18. E. Gerjuoy, S. Stein, Phys. Rev. **97**, 1671 (1955)
19. Yu. D. Oksyuk, Sov. Phys. J. Exp. Theor. Phys. **22**, 873 (1966)
20. J.B. Fisk, Phys. Rev. **49**, 167 (1936)
21. M.A. Ridenti, L.L. Alves, V. Guerra, J. Amorim, Plasma Sources Sci. Technol. **24**, 035002 (2015)
22. K.P. Huber, G. Herzberg, *Molecular Spectra and Molecular Structure. IV. Constants of Diatomic Molecules* (Springer, New York, 1979)
23. DUTTON database, www.lxcat.net, retrieved on June 2014
24. LAPLACE database, www.lxcat.net, retrieved on June 2014
25. R.A. Nielsen, N.E. Bradbury, Phys. Rev. **51**, 69 (1937)
26. A. Doehring, Z. Naturforsch. **7A**, 253 (1952)
27. P. Herreng, Cahiers Phys. **38**, 1 (1952)
28. L. Frommhold, Fortschr. Phys. **1**, 597 (1964)
29. H. Schlumbohm, in *Proc. Fourth International Conference on Ionization Phenomena in Gases*, edited by N.R. Nilsson (North-Holland Publishing Company, Amsterdam, 1960), Vol. 1, 1B 127
30. R.D. Hake, A.V. Phelps, Phys. Rev. **158**, 70 (1967)
31. M.S. Naidu, A.N. Prasad, J. Phys. D **3**, 957 (1970)
32. I. Fleming, D.R. Gray, J.A. Rees, J. Phys. D **5**, 291 (1972)
33. D.R. Nelson, F.J. Davis, J. Chem. Phys. **57**, 4079 (1972)
34. H.L. Brose, Philos. Mag. **1**, 536 (1925)
35. R.W. Crompton, M.T. Elford, Aust. J. Phys. **26**, 771 (1973)
36. I.D. Reid, R.W. Crompton, Aust. J. Phys. **33**, 215 (1980)

37. W. Roznerski, K. Leja, J. Phys. D **17**, 279 (1984)
38. B.-H. Jeon, Y. Nakamura, J. Phys. D **31**, 2145 (1998)
39. V. Lisovskiy, J.-P. Booth, K. Landry, D. Douai, V. Cassagne, V. Yegorenkov, J. Phys. D **39**, 660 (2006)
40. L.G.H. Huxley, R.W. Crompton, C.H. Bagot, Aust. J. Phys. **1**, 303 (1959)
41. J.A. Rees, Aust. J. Phys. **18**, 41 (1965)
42. M.A. Harrison, R. Geballe, Phys. Rev. **91**, 1 (1953)
43. L. Frommhold, Z. Phys. **160**, 554 (1960)
44. A.N. Prasad, J.D. Craggs, Proc. Phys. Soc. London **77**, 385 (1961)
45. J. Dutton, F. Llewellyn-Jones, G.B. Morgan, Nature **198**, 680 (1963)
46. J.B. Freely, L.H. Fisher, Phys. Rev. **133**, A304 (1964)
47. D.A. Price, J. Lucas, J.L. Moruzzi, J. Phys. D **5**, 1249 (1972)
48. B.C. O'Neill, J.D. Craggs, J. Phys. B **6**, 2625 (1973)
49. D.A. Price, J. Lucas, J.L. Moruzzi, J. Phys. D **6**, 1514 (1973)
50. R.J. Corbin, L. Frommhold, Phys. Rev. A **10**, 2273 (1974)
51. P.A. Chatterton, J.D. Craggs, J. Electron. Control **11**, 425 (1971)
52. R. Grünberg, Z. Naturforsch. **24a**, 1039 (1969)
53. C.S. Lakshminarasimha, J. Lucas, R.A. Snelson, Proc. IEE **12**, 10 (1975)
54. R.R. Laher, F.R. Gilmore, J. Phys. Chem. Ref. Data **19**, 277 (1990)
55. R.I. Hall, S. Trajmar, J. Phys. B **8**, L293 (1975)
56. P.D. Burrow, J. Chem. Phys. **59**, 4922 (1973)
57. L. Vejby-Christensen, D. Kella, D. Mathur, H.B. Pedersen, H.T. Schmidt, L.H. Andersen, Phys. Rev. A **53**, 2371 (1996)
58. G.D. Stancu, O. Leroy, P. Coche, K. Gadonna, V. Guerra, T. Minea, L.L. Alves, J. Phys. D (submitted 2016)
59. P. Coche, L.L. Alves, V. Guerra, K. Gadonna, G.D. Stancu, O. Leroy, T. Minea, in *32nd International Conference on Phenomena in Ionized Gases, Iasi, Romania* (2015), pp. P4–39
60. L.L. Alves, L. Marques, C.D. Pintassilgo, G. Wattieaux, E. Es-sebbar, J. Berndt, E. Kovacević, N. Carrasco, L. Boufendi, G. Cernogora, Plasma Sources Sci. Technol. **21**, 045008 (2012)
61. M.L. da Silva, V. Guerra, J. Loureiro, P. Sá, J. Chem. Phys. **348**, 187 (2008)
62. V. Guerra, J. Loureiro, Plasma Sources Sci. Technol. **6**, 373 (1997)
63. P. Coche, V. Guerra, L.L. Alves, J. Phys. D (in press 2016)
64. S.A. Self, H.N. Ewald, Phys. Fluids **9**, 2486 (1966)
65. C.M. Ferreira, A. Ricard, J. Appl. Phys. **54**, 2261 (1983)
66. S. Dap, O. Leroy, J. Andrieu, C. Boisse-Laporte, P. Leprince, G.D. Stancu, T. Minea, Plasma Sources Sci. Technol. **24**, 065006 (2015)
67. Specair, www.specair-radiation.net
68. P.W. Erdman, E.C. Zipf, J. Chem. Phys. **87**, 4540 (1987)
69. H.M. Katsch, A. Tewes, E. Quandt, A. Goehlich, T. Kawetzki, H.F. Dbele, J. Appl. Phys. **88**, 6232 (2000)
70. M. Tashiro, K. Morokuma, J. Tennyson, Phys. Rev. A **73**, 052707 (2006)